Geophys. J. Int. (2003) **152,** F1–F7

FAST TRACK PAPER

Teleseismic P_n arrivals: influence of mantle velocity gradient and crustal scattering

L. Nielsen,[1] H. Thybo,[1] I. B. Morozov,[2] S. B. Smithson[2] and L. Solodilov[3]

[1] *Geological Institute, University of Copenhagen,* DK-1350 *Copenhagen K, Denmark. E-mail: ln@geo.geol.ku.dk*
[2] *Department of Geology and Geophysics, University of Wyoming, Laramie, WY* 82071-3006, *USA*
[3] *GEON Center, Moscow,* 119034 *Russia*

Accepted 2002 October 23. Received 2002 October 16; in original form 2002 May 23

Downloaded from https://academic.oup.com/gji/article/152/2/F1/2027597 by guest on 02 February 2022

SUMMARY

Teleseismic P_n phases with a long, high-amplitude coda, are observed to offsets >3000 km along the Peaceful Nuclear Explosion seismic profiles Quartz and Ruby. For the high-frequency (>5 Hz) part of the Quartz data, which is shown here, coda lengths of more than 10 s can be visually observed in the seismic sections. We interpret the teleseismic P_n arrivals as multiple sub-Moho refractions (whispering-gallery phases), which travel over large distances due to a positive upper-mantle velocity gradient. The coda of these arrivals is explained by lower crustal scattering of the whispering-gallery phases from the mantle. The modelling is based on calculation of reflectivity and 2-D visco-elastic finite-difference synthetic seismograms. Our models are in agreement with other deep seismic data from continental areas, which typically show a reflective lower crust and an almost transparent uppermost mantle. The lower crustal heterogeneity is described by von Karman distribution with a standard deviation of 0.5 km s^{-1} for the *P*-wave velocity and correlation lengths of 2.4 km (horizontally) and 0.6 km (vertically). The positive vertical upper-mantle velocity gradient of ~0.004 km s^{-1} km^{-1}, which is characteristic for profile Quartz, forms a waveguide which gives rise to the teleseismic P_n. It is not necessary to include upper-mantle heterogeneity in order to explain the characteristics of this arrival.

Key words: crust, nuclear explosions, refraction seismology, scattering, seismic-wave propagation, upper-mantle.

1 INTRODUCTION

Peaceful Nuclear Explosion (PNE) seismic profiling conducted in the former Soviet Union (e.g. Egorkin *et al.* 1984) has recorded high-frequency seismic arrivals to extreme offsets (up to 4000 km) from the seismic sources. The teleseismic (or long-range) P_n arrivals are observed to >3000 km offset along PNE seismic profiles Quartz and Ruby (Fig. 1). They provide unique information about the fine-scale structure of the crust-upper-mantle system because they carry a long coda with a relatively strong high-frequency (>5 Hz) content. Two fundamentally different explanations have been offered for the origin of the teleseismic P_n phase. Based on reflectivity calculations (3-D calculations for 1-D layered structure) and 2-D elastic finite-difference (FD) modelling, Tittgemeyer *et al.* (1996), Ryberg & Wenzel (1999) and Ryberg *et al.* (2000) argue that the scattered arrivals of the teleseismic P_n are caused by an inhomogeneous zone between the Moho and about 100 km depth, which acts as a waveguide to the high-frequency part of the seismic wavefield. In contrast to these interpretations, Morozov *et al.* (1998), Morozov & Smithson (2000) and Morozov (2001) suggest that the teleseismic P_n should be understood as whispering-gallery phases, which propagate as multiple refractions along the Moho due to a positive upper-mantle velocity gradient. Based on 3-D energy balance consideration and coda decay modelling, Morozov & Smithson (2000) argue that the coda of the teleseismic P_n arrivals could be explained solely by crustal scattering.

We present new results based on reflectivity modelling and 2-D visco-elastic FD modelling. Our results show that the pronounced coda of the teleseismic P_n may be explained by lower crustal heterogeneities that are likely to be found in continental areas. The vertical velocity gradient of the upper-mantle controls the key characteristics of the observed teleseismic P_n phase.

2 KEY OBSERVATIONS

The arrival times of the primary *P* waves in the Quartz PNE seismic sections (Fig. 1) constrain the overall velocity structure along the profile (e.g. Morozova *et al.* 1999). Between ~300 and ~1000 km

© 2003 RAS

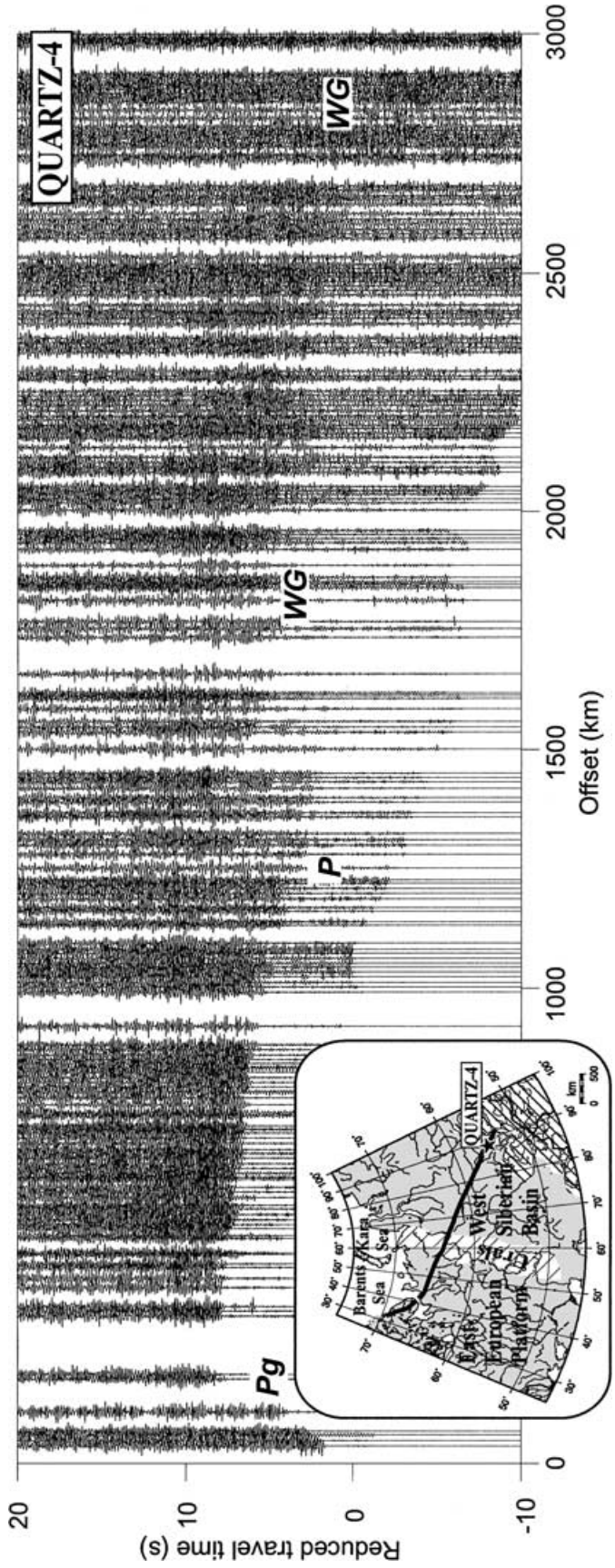

Figure 1. Trace-normalized and high-pass filtered (>5 Hz) seismic section of PNE Quartz 4 plotted in reduced traveltime format (reduction velocity: 8.0 km s^{-1}). Pg: refracted crustal waves. P: primary mantle arrival. WG: whispering-gallery phase (teleseismic P_n). Inset shows PNE locations and major tectonic features.

Downloaded from https://academic.oup.com/gji/article/152/2/F1/2027597 by guest on 02 February 2022

offset the apparent velocity of the primary *P* waves varies between 8.0 km s^{-1} and 8.2 km s^{-1}; beyond 1000 km offset it increases to more than 8.4 km s^{-1}. The amplitude of the primary *P* arrival decreases significantly near ∼1500 km offset due to the existence of proposed low-velocity zones in the upper-mantle (Morozova *et al.* 1999).

The teleseismic P_n phase, which must be primarily propagating in the uppermost mantle, is clearly observed from ∼1200 km offset where it detaches from the faster first arriving *P*-waves which travel deeper in the upper-mantle (Fig. 1). Its traveltime is equivalent to whispering-gallery arrivals, which propagate as multiple refractions along the Moho (Morozov *et al.* 1998). Important characteristics of the teleseismic P_n are: (1) an incoherent, high-amplitude coda which dominates the high-frequency part of the seismic records for several seconds (Tittgemeyer *et al.* 1996), possibly up to ∼200 s (Morozov & Smithson 2000), and (2) an apparent velocity which gradually increases from ∼8.0 km s^{-1} at ∼1200 km to >8.4 km s^{-1} beyond ∼2000 km offset (*cf.* Morozov *et al.* 1998). At 500–1000 km offset, clear and strong high-amplitude arrivals also trail the primary *P* phase.

3 SEISMIC WAVEFORM MODELLING

Previous modelling has shown that velocity fluctuations in the continental lower crust may explain the codas often observed for lower crustal wide-angle reflections (e.g. Levander & Holliger 1992; Enderle *et al.* 1997). We test whether lower crustal scattering can also explain the high-frequency (>5 Hz) part of the teleseismic P_n coda. We first examine 1-D models in which the lower crust from 15 km to 40 km depth contains small-scale, random velocity fluctuations. The fluctuations are superimposed on a background velocity model in which the 15–30 km depth range has a constant *P*-wave velocity of 6.5 km s^{-1}, and the Moho is represented by a transition zone from 30 km to 40 km depth where the velocity increases from 6.5 km s^{-1} to 8.0 km s^{-1}. In the models of Figs 2(a) and (b), each random velocity layer is 250 m thick and the *P*-wave velocity fluctuations are ±0.5 km s^{-1}. Fluctuations with such amplitudes have previously been suggested for the lower crust in order to explain the coda of supercritical *PmP* reflections from the Moho and may correspond to felsic rocks intermixed with mafic material (e.g. Enderle *et al.* 1997). *S*-wave velocity is related to *P*-wave velocity assuming a Poisson's ratio of 0.25, and density is linked to velocity using the linear relation of Birch (1961). The two models in Fig. 2 only differ in the choice of velocity structure below Moho. In Fig. 2(a) we have adopted a smoothed version of the average upper-mantle velocity model for profile Quartz as estimated from detailed traveltime modelling (Morozova *et al.* 1999); in Fig. 2(b) the increase in upper mantle velocity with depth is low, from 8.0 km s^{-1} at 40 km depth to 8.2 km s^{-1} at 150 km depth (*cf.* Ryberg *et al.* 2000). The seismic section (Fig. 2c) calculated for the model of Fig. 2(a) shows: (1) a clear teleseismic P_n phase with an incoherent coda of several seconds duration from ∼1200 km offset; (2) the apparent velocity of the teleseismic P_n gradually increases with offset; (3) at 500–1000 km offset a high-amplitude wave train of scattered arrivals is clearly evident behind the primary *P* arrivals; and (4) a gradual increase in the apparent velocity of the primary *P*-wave to >8.4 km s^{-1} is visible until the amplitude of this phase decreases strongly at ∼1500 km offset. Thus, the calculated seismic section of Fig. 2(c) matches all key observations regarding the teleseismic P_n. However, in this modelled section the first few wiggles of the teleseismic P_n generally have higher amplitudes than the coda of this arrival, which is not the case in the real data. The model of Fig. 2(b) cannot explain the observations (Fig. 2d). The primary P_n has a too low apparent velocity and its amplitude does not decrease markedly until ∼2000 km offset. Furthermore, the teleseismic P_n does not separate clearly from the primary P_n phase until ∼1700 km offset, and the coda is too weak (Fig. 2d). The model in Fig. 2(b) is unable to match the observed traveltimes for the first arriving *P*-waves from the upper-mantle. In fact, this mismatch is a common feature for all low-gradient upper-mantle models that have been used for explaining the teleseismic P_n by upper-mantle heterogeneity (e.g. Ryberg & Wenzel 1999; Ryberg *et al.* 2000).

Crustal heterogeneities most likely are 3-D, and scattering of long-range arrivals is a 3-D process (Morozov & Smithson 2000). However, 3-D full waveform calculations in large upper-mantle models are not feasible with present-day computers. Hence, we cannot quantify which part of the spatial propagation effects that are not correctly accounted for. However, our previous experience is that 2-D finite-difference modelling results in longer codas than reflectivity calculations for given upper-mantle heterogeneity parameters (Nielsen *et al.* 2001, 2002). In order to assess the effects of horizontal heterogeneity, we here present the results of 2-D visco-elastic FD modelling using the algorithm described by Robertsson *et al.* (1994), although this approach does not result in a correct 3-D description of amplitude decay with offset. We calculate synthetic seismograms for 2000 km wide and 240 km deep models, which are defined on a grid with a constant horizontal and vertical grid spacing of 75 m. This assures at least 5 grid points per *S*-wavelength for frequencies up to 10 Hz in the 2-D models (Figs 3a and b). The synthetic seismograms are calculated in time steps of 3.1 ms in order to maintain stability of the FD algorithm. Undesired reflections from the sides and bottom of the model are damped by a 30 km wide highly attenuating zone (Qp = Qs = 2), which is padded around the model. In the 2-D case, we describe the fluctuations below 15 km depth by a von Karman distrubution with a Hurst number of 0.3 (*cf.* Holliger & Levander 1992). The horizontal and vertical correlation lengths are 2.4 km and 0.6 km, respectively. The standard deviation of the 2-D *P*-wave fluctuations is 0.5 km s^{-1}, and it is assured that none of the fluctuations exceed ±10 per cent of the background velocity value. The assumed Poisson's ratio and the velocity-density relation are identical to the 1-D cases. The 2-D synthetic section (Fig. 3c) provides a good fit to all key characteristics made out to 2000 km. The kinematics of the first arriving *P*-waves and the whispering-gallery arrival are reproduced, and the extensive, high-amplitude codas of these phases are matched. At short offsets (<250 km), the 2-D model gives rise to lower crustal reflectivity and supercritical *PmP* coda (Fig. 4). Such features are often observed in continental wide-angle sections (e.g. Enderle *et al.* 1997).

Small deviations between the absolute travel times of the modelled phases and the observed phases exist, because our simple stratified background model cannot account for all the variations in the velocity field along profile Quartz.

4 DISCUSSION

Comparisons between observed and modelled seismic sections show that the key characteristics of the teleseismic P_n phase may be explained by whispering-gallery phases that are influenced by scattering in the lower crust. These results are contrary to the findings of Ryberg & Wenzel (1999) and Ryberg *et al.* (2000), who explain the teleseismic P_n by a ∼100 km thick inhomogeneous layer below Moho which acts as a waveguide to the high-frequency part of the

Downloaded from https://academic.oup.com/gji/article/152/2/F1/2027597 by guest on 02 February 2022

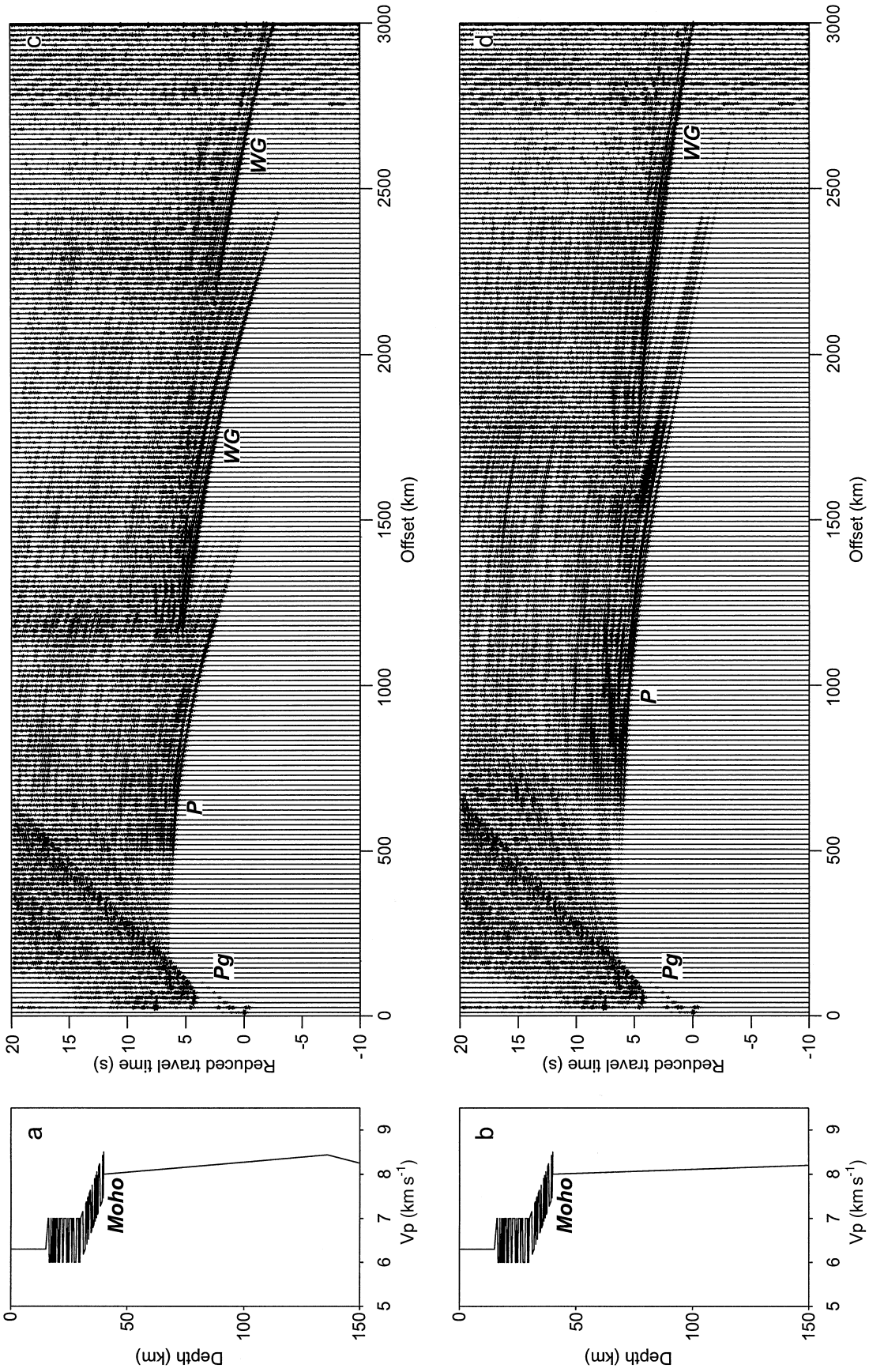

Figure 2. (a) 1-D model including random velocity (±0.5 km s^{-1}) layers of 250 m thickness from 15 to 40 km depth. Below Moho the velocity profile is a smoothed version of the average velocity structure along profile Quartz (*cf.* Morozova *et al.* 1999). (b) Same as (a) for the crust, but below Moho the velocity profile is taken from Ryberg *et al.* (2000). (c) Synthetic seismogram montage calculated for the model in (a) using the reflectivity method of Fuchs & Müller (1971). (d) Reflectivity seismic section calculated for the model in (b). The trace-normalized, high-pass filtered (>5 Hz) seismic sections of (c) and (d) are calculated using a Ricker wavelet as the source and plotted in reduced traveltime format (reduction velocity: 8.0 km s^{-1}). Pg: refracted crustal waves. P: primary mantle arrival. WG: whispering-gallery (teleseismic P_n) arrivals. All arrivals in the synthetic seismograms are ~2 s early compared to the observed data because no low-velocity sedimentary layer is included in the 1-D models.

Downloaded from https://academic.oup.com/gji/article/152/2/F1/2027597 by guest on 02 February 2022

© 2003 RAS, *GJI*, **152,** F1–F7

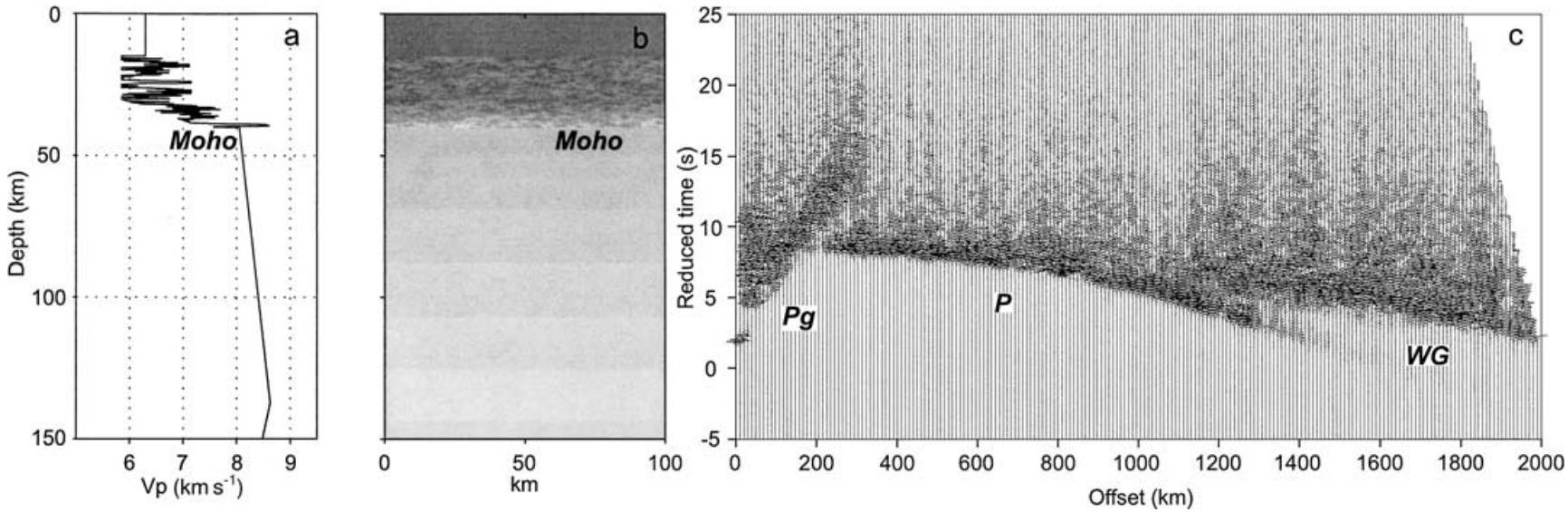

Figure 3. (a) 1-D *P*-wave velocity profile extracted from the 2000 km wide 2-D model of which the first 100 km are shown in (b). The fluctuations from 15 to 40 km depth are described by a von Karman distribution function with a Hurst number of 0.3 (*cf.* Holliger & Levander 1992). In the upper 5 km of the model we have applied low Qp- and Qs-values of 20 and 12, respectively, in order to take into account the inelastic damping effects of faulted basement, sedimentary strata and surface topography. From 5 to 15 km depth Qp and Qs are 500 and 300, respectively. Below 15 km depth we have constant Qp- and Qs-values of 1000 and 600. Sphericity of the Earth is accounted for by applying the flat-earth transformations (Aki & Richards 1980). (c) Trace-normalized seismic section calculated for the 2-D visco-elastic model plotted in reduced traveltime format (reduction velocity: 8.0 km s^{-1}). The source is a Ricker wavelet with a central frequency of 5 Hz. High-pass filter (>5 Hz) applied. Pg: refracted crustal waves. P: primary mantle arrival. WG: whispering-gallery (teleseismic P_n) arrivals.

Downloaded from https://academic.oup.com/gji/article/152/2/F1/2027597 by guest on 02 February 2022

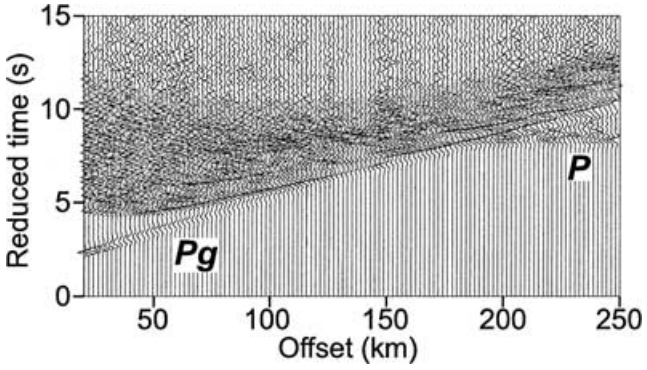

Figure 4. 2-D synthetic, trace-normalized arrivals at offsets <250 km for the model of Fig. 3. No filtering applied. Shaded area shows reflectivity and *PmP* coda produced by the lower crustal scatterers. Pg: refracted crustal waves. P: primary mantle arrival.

seismic wavefield. They conclude that crustal scattering only has minor influence on the coda characteristics of the teleseismic P_n. However, their modelling is based on a background velocity model in which the overall upper-mantle vertical velocity gradient is very small (Fig. 2b). For such a low vertical upper-mantle velocity gradient, we also find that whispering-gallery phases influenced by lower crustal scattering cannot account for neither the observed kinematics nor for the coda characteristics of the teleseismic P_n (Fig. 2c).

However, such a low upper-mantle velocity gradient is not representative of the velocity structure below profile Quartz (Morozova *et al.* 1999). Therefore, none of the synthetics of Ryberg & Wenzel (1999) and Ryberg *et al.* (2000) match the first arrival traveltimes observed along profile Quartz. Our preferred models (Figs 2a and 3) fit the observed first arrival traveltimes as well as the kinematics and coda characteristics of the teleseismic P_n.

The coda of the teleseismic P_n dominates the high-frequency part of the PNE data, but it also has a significant low-frequency content (Morozov & Smithson 2000). The positive upper-mantle velocity gradient below profiles Quartz and Ruby explains the propagation of both the high- and low-frequency arrivals to teleseismic distances. However, the low-frequency part of the wavefield is less sensitive to the short-scale lower crustal heterogeneity than the high-frequency part.

Our preferred velocity model of the crust and uppermost mantle for profile Quartz agrees with typical observations in high-resolution, deep normal-incidence seismic data collected in continental areas regarding a reflective lower crust and an almost transparent upper mantle down to ~20–25 s traveltime (e.g. Bois & ECORS Working Group 1991; MONA LISA Working Group 1997). Due to such observations it is often argued that the lower crust is highly heterogeneous and that the uppermost mantle is more homogeneous. However, based on these observations alone one cannot rule out fine-scale heterogeneity of the uppermost mantle. Tittgemeyer *et al.* (1999) show that upper-mantle velocity fluctuations can be tuned to not cause backscattering at short offsets from the seismic source by restricting the fluctuations to certain scale lengths. Our modelling results show that lower crustal heterogeneity alone may explain the coda characteristics of the teleseismic P_n phase. However, we do not conclude that heterogeneity does not exist in the uppermost mantle.

Investigations of long-range, controlled-source seismic data collected around the globe have revealed an inhomogeneous zone below ~100 km depth in continental mantle (Thybo & Perchuć 1997). This scattering zone has also been identified along PNE profile Kraton in Siberia (Nielsen *et al.* 2002). The scattered arrivals originating from this zone are observed directly behind the first arrivals from ~800–1400 km offset and do not interfere with the teleseismic P_n phase.

We have restricted ourselves to modelling of lower crustal velocity fluctuations. Inhomogeneities and large fault systems in the upper crust, stratification of thick sedimentary basins and surface topography will give rise to additional scattering of the seismic wavefield and contribute further to the coda of the teleseismic P_n (e.g. Morozov *et al.* 1998; Morozov & Smithson 2000; Revenaugh 1995).

5 CONCLUSIONS

Based on reflectivity modelling and 2-D visco-elastic FD calculations we find that: (1) teleseismic P_n arrivals propagating as whispering-gallery phases along the crust-mantle boundary may be observed to large distances from the source location (>3000 km) if the uppermost mantle is characterized by a positive vertical velocity gradient, as observed along profile Quartz; (2) heterogeneous material likely to constitute the lower crust may contribute significantly to the high-frequency coda of the teleseismic P_n phase; (3) the key characteristics of the teleseismic P_n phase highly depend on the velocity gradient of the upper-mantle and, therefore, this phase may exhibit regional variability; (4) it is not necessary to include a special upper-mantle scattering waveguide in the form of a thick heterogeneous zone below the Moho in order to explain the nature of the teleseismic P_n.

ACKNOWLEDGMENTS

This study was financed by the Carlsberg Foundation and the Danish Natural Science Research Council I. B. M. was sponsored in part by the US Defense Threat Reduction Agency Grant DSWA01-98-0015. The waveform calculations were made on the computer systems of the Danish Center for Scientific Computing (DCSC), Denmark. Johan Robertsson provided the visco-elastic FD codes.

REFERENCES

Aki, K. & Richards, P.G., 1980. *Quantitative Seismology: Theory and Methods,*I–II, W. H. Freeman and Company, San Francisco.

Birch, F., 1961. The velocity of compressional waves in rocks to 10 kilobars, Part 2, *J. Geophys. Res.,* **66,** 2199–2224.

Bois, C. & ECORS Working Group, 1991. Late- and post-orogenic evolution of the crust studied from ECORS deep seismic profiles, in *Continental Lithosphere: Deep Seismic Reflections,Geodynamics Series,* pp. 59–68, eds Meissner, R., Brown, L., Dürbaum, H.-J., Franke, W., Fuchs, K. & Seifert, F., American Geophysical Union, Washington DC.

Egorkin, A.V., Zuganov, S.K. & Chernyshov, N.M., 1984. The upper mantle of Siberia, *Proceedings of the 27th International Geological Congress,* **8,** 29–56.

Enderle, U., Tittgemeyer, M., Itzin, M., Prodehl, C. & Fuchs, K., 1997. Scales of structure in the lithosphere—Images of processes, *Tectonophysics,* **275,** 165–198.

Fuchs, K. & Müller, G., 1971. Computation of Synthetic Seismograms with the Reflectivity Method and Comparison with Observations, *Geophys. J. R. astr. Soc.,* **23,** 417–433.

Holliger, K. & Levander, A.R., 1992. A stochastic view of lower crustal fabric based on evidence from the Ivrea Zone, *Geophys. Res. Lett.,* **19,** 1153–1156.

Levander, A.R. & Holliger, K., 1992. Small-scale heterogeneity and large-scale velocity structure of the continental crust, *J. geophys. Res.,* **97,** 8797–8804.

Downloaded from https://academic.oup.com/gji/article/152/2/F1/2027597 by guest on 02 February 2022

MONA LISA Working Group, 1997. Deep seismic investigations of the lithosphere in the south-eastern North Sea, *Tectonophysics,* **269,** 1–19.

Morozov, I.B., 2001. Comment on 'High-frequency wave propagation in the uppermost mantle' by T. Ryberg & F. Wenzel, *J. geophys. Res.,* **106,** 30 715–30 718.

Morozov, I.B. & Smithson, S.B., 2000. Coda of Long-Range Arrivals from Nuclear Explosions, *Bull. seism. Soc. Am.,* **90,** 929–939.

Morozov, I.B., Morozova, E.A., Smithson, S.B. & Solodilov, L.N., 1998. On the Nature of the Teleseismic P_n Phase Observed on the Ultralong-Range Profile 'Quartz,' Russia, *Bull. seism. Soc. Am.,* **88,** 62–73.

Morozova, E.A., Morozov, I.B. & Smithson, S.B., 1999. Heterogeneity of the uppermost mantle beneath Russian Eurasia from the ultra-long-range profile QUARTZ, *J. geophys. Res.,* **104,** 20 329–20 348.

Nielsen, L., Thybo, H. & Egorkin, A., 2001. Constraints on reflective bodies below the 8° discontinuity from reflectivity modelling, *Geophys. J. Int.,* **145,** 759–770.

Nielsen, L., Thybo, H. & Egorkin, A., 2002. Implications of seismic scattering below the 8° discontinuity along PNE profile Kraton, *Tectonophysics,* **358,** 135–150.

Revenaugh, J., 1995. The contribution of topographic scattering to teleseismic coda in Southern California, *Geophys. Res. Lett.,* **22,** 543–546.

Robertsson, J.O.A., Blanch, J.O. & Symes, W.W., 1994. Viscoelastic finite-difference modeling, *Geophysics,* **59,** 1444–1456.

Ryberg, T. & Wenzel, F., 1999. High-frequency wave propagation in the uppermost mantle, *J. geophys. Res.,* **104,** 10 655–10 666.

Ryberg, T., Tittgemeyer, M. & Wenzel, F., 2000. Finite difference modelling of *P*-wave scattering in the upper mantle, *Geophys. J. Int.,* **141,** 787–800.

Thybo, H. & Perchuć, E., 1997. The Seismic 8° Discontinuity and Partial Melting in Continental Mantle, *Science,* **275,** 1626–1629.

Tittgemeyer, M., Wenzel, F., Fuchs, K. & Wenzel, F., 1996. Wave propagation in a Multiple Scattering Upper Mantle—Observation and Modelling, *Geophys. J. Int.,* **127,** 492–502.

Tittgemeyer, M., Wenzel, F., Ryberg, T. & Fuchs, K., 1999. Scales of Heterogeneities in the Continental Crust and Upper Mantle, *Pure appl. Geophys.,* **156,** 29–52.

Downloaded from https://academic.oup.com/gji/article/152/2/F1/2027597 by guest on 02 February 2022